Geophysical Journal International

Geophys. J. Int. (2012) **191,** 1135–1151 doi: 10.1111/j.1365-246X.2012.05677.x

Bayesian inversion of marine CSEM data with a trans-dimensional self parametrizing algorithm

Anandaroop Ray and Kerry Key

Scripps Institution of Oceanography, La Jolla, CA, USA. E-mail: anray@ucsd.edu

Accepted 2012 September 10. Received 2012 September 3; in original form 2012 June 7

SUMMARY

The posterior distribution of earth models that fit observed geophysical data convey information on the uncertainty with which they are resolved. From another perspective, the non-uniqueness inherent in most geophysical inverse problems of interest can be quantified by examining the posterior model distribution converged upon by a Bayesian inversion. In this work we apply a reversible jump Markov chain Monte Carlo method to sample the posterior model distribution for the anisotropic 1-D seafloor conductivity constrained by marine controlled source electromagnetic data. Unlike conventional gradient based inversion approaches, our algorithm does not require any subjective choice of regularization parameter, and it is self parametrizing and trans-dimensional in that the number of interfaces with a resistivity contrast at depth is variable, as are their positions. A synthetic example demonstrates how the algorithm can be used to appraise the resolution capabilities of various electromagnetic field components for mapping a thin resistive reservoir buried beneath anisotropic conductive sediments. A second example applies the method to survey data collected over the Pluto gas field on the Northwest Australian shelf. A benefit of our Bayesian approach is that subsets of the posterior model probabilities can be selected to test various hypotheses about the model structure, without requiring further inversions. As examples, the subset of model probabilities can be viewed for models only containing a certain number of layers, or for models where resistive layers are present between a certain interval as suggested by other geological constraints such as seismic stratigraphy or nearby well logs.

Key words: Inverse theory; Electromagnetic theory; Marine electromagnetics; Australia.

1 INTRODUCTION

The ability of marine controlled-source electromagnetic (CSEM) data to detect thin resistive layers such as hydrocarbon formations trapped in conductive sediments is now well-known due to more than a decade of research conducted in conjunction with the commercialization of CSEM technologies (e.g. Ellingsrud *et al.* 2002; Um & Alumbaugh 2007; Constable 2010). Given a CSEM data set, the inverse problem is to find a resistivity model compatible with the data. This non-linear ill-posed inverse problem can be tackled in a number of ways. The traditional approaches used during the past few decades for various EM geophysics applications have relied on regularization methods that serve to stabilize the problem, usually through the use of norms that penalize the model roughness or deviations from a preferred model (e.g. Constable *et al.* 1987; Newman & Alumbaugh 2000; Abubakar *et al.* 2008). Though highly efficient and well understood, these gradient based optimization methods only provide a single smooth model as a result, or provide a suite of smooth models as a function of data misfit. While such results can be considered robust in the sense that the smoothness constraint tends to eliminate unnecessary or spurious features and retains only those smooth features required to fit the data, these methods have a very narrow view of the full range of models compatible with the data. Furthermore, questions about the resolution of the resulting inverse models remain unanswered.

A solution to this problem is to utilize Bayesian methods to characterize model resolution in terms of marginal probability density functions (PDFs) for each model parameter (e.g. Sen & Stoffa 1995). Since Bayesian probability is a statement of information, it is natural to postulate geophysical inversion in a Bayesian framework. Inversion thus implies sampling a posterior model distribution, which depends on available prior information on likely models and the likelihood of the data fit for sampled models. The posterior distribution of model parameters conveys information on the uncertainty with which they are resolved. From another perspective, the non-uniqueness inherent in most geophysical problems of interest can be quantified by examining the posterior model distribution.

Our study is not the first to apply Bayesian methods for 1-D inversion of marine CSEM problems. One of the earliest applications focused on joint inversion of CSEM and seismic data in order to improve estimates of reservoir properties (Hou *et al.* 2006; Chen *et al.*

2007). Trainor-Guitton & Hoversten (2011) use a sampling scheme which involves both the Metropolis-Hastings algorithm and slice sampling (Neal 2003) to improve convergence upon the distribution of solution models. Buland & Kolbjornsen (2012) apply the Metropolis-Hastings algorithm (Hastings 1970) to invert marine CSEM data together with magnetotelluric (MT) data to constrain the range of likely resistivities as a function of depth.

While these inversions have indeed been probabilistic, they have not addressed the issue of model selection, or scalability of the model space. That is to say, either the number of layers and their depths have been fixed *a priori* using only a few parameters, or the number of depth intervals is very large to allow for more structural detail (requiring considerably more computational effort). Having too few or too many parameters will bias the inversion results (Dettmer *et al.* 2010). Tompkins *et al.* (2011) address the issue of model space scalability for the marine CSEM problem by using either a principle component analysis approach or singular value decomposition to transform their model domain. This may result in a more efficient search since the model space is greatly reduced (Collins & Fishman 1995), and has similarly been applied to geo-acoustic inversion (Dosso & Dettmer 2011). However, the approach of Tompkins *et al.* (2011) is not Bayesian and requires a starting regularization as well as subjective layer parametrization. Gunning *et al.* (2010) developed a 'Bayesianized' parametric bootstrap method that splits layers to create resolution at depths statistically justified by the CSEM data.

Our approach is to essentially use nothing more complicated than Bayes' theorem (Bayes 1763) itself, and the idea of 'Bayesian parsimony' which states that the evidence term in Bayes' theorem prefers models with simpler model parametrizations (Dettmer *et al.* 2010). To this end we apply the reversible jump Markov Chain Monte Carlo (RJ-MCMC) method to characterize model uncertainty for marine CSEM data. This approach was first introduced to the statistics community for change point analysis by Green (1995) and deals with a variable number of unknowns, which in our case are the number and positions of the model layers and their resistivities. The RJ-MCMC method has found widespread use in a diverse number of fields from genetics (Huelsenbeck *et al.* 2004) to automated surveillance (Smith *et al.* 2005). In the geophysical realm, Malinverno (2002) has applied it to DC resistivity data inversion and more recently Agostinetti & Malinverno (2010) and Bodin *et al.* (2012) have used it for seismic receiver function analysis. A recent application to airborne electromagnetic (EM) can be found in Minsley (2011). RJ-MCMC methods are often said to be 'trans-dimensional', where trans-dimensionality implies that the number of model parameters is variable. The algorithm we follow has been used for the geo-acoustic problem (Dettmer *et al.* 2010) and seismic surface wave tomography (Bodin & Sambridge 2009), using the 'partition modelling' approach outlined by Bodin & Sambridge (2009).

The manner in which this algorithm avoids regularization yet provides reasonable solutions is elegantly simple. The results of the inversion, as in any Bayesian framework, are not limited to a single 'best-fit' solution. Instead, the algorithm provides a distribution of model solutions, the large majority of which fit the data to within its uncertainty. The non-uniqueness inherent in most geophysical inverse problems due to both the physics of the problem and a finite set of noisy observations implies that there are an infinite number of models that fit the data. However, some parts of the model space are more frequently required by models that fit the data than other parts of the model space. It is these parts of the model space which are deemed to be more probable (Backus 1988; Tarantola 2005). Since the model space is often high-dimensional, the ensemble of models can be conveniently viewed via marginal distributions of the parameters of interest (e.g. Sen & Stoffa 1995).

Here we present the theory for a trans-dimensional RJ-MCMC with an adaptation that mixes local and global steps in the model space to ensure thorough sampling of the model space. We then proceed with two example applications for marine CSEM inversion. The first is a resolution test for resistivity anisotropy in a model of a thin resistive layer representing an offshore hydrocarbon reservoir and the second is an application to CSEM survey data collected over the Pluto gas field in the Northwest Shelf of Australia.

2 THEORY AND ALGORITHM

2.1 Anisotropic forward modelling

The analytic expressions for the EM fields in media that are transversely isotropic about the vertical (TIV) due to electric and magnetic dipole transmitters are given in appendix F of Løseth & Ursin (2007). As an illustrative example, we provide here the integral transform for the radial electric field due to a horizontal electric dipole (HED) at an azimuth β and range r from the dipole, normalized by the source dipole moment:

$$E_r = -\frac{1}{4\pi}\cos\beta\left[\mathcal{I}_0^{\mathrm{TM}} + \frac{1}{r}\left(\mathcal{I}_1^{\mathrm{TE}} - \mathcal{I}_1^{\mathrm{TM}}\right)\right], \tag{1}$$

where

$$\mathcal{I}_0^{\mathrm{TM}} = \int_0^\infty \mathrm{d}k_r\, k_r J_0(k_r r) g^{\mathrm{TM}}(p_{zII}), \tag{2}$$

$$\mathcal{I}_1^{\mathrm{TE}} = \int_0^\infty \mathrm{d}k_r\, J_1(k_r r) g^{\mathrm{TE}}(p_{zI}), \tag{3}$$

$$\mathcal{I}_1^{\mathrm{TM}} = \int_0^\infty \mathrm{d}k_r\, J_1(k_r r) g^{\mathrm{TM}}(p_{zII}). \tag{4}$$

Table 1. Modes present in the various EM field components produced by each of the four fundamental electric and magnetic dipoles sources when embedded in 1-D layered media.

Component	HED	VED	HMD	VMD
E_r	TE,TM	TM	TE,TM	
E_β	TE,TM		TE,TM	TE
E_z	TM	TM	TM	
H_r	TE,TM		TE,TM	TE
H_β	TE,TM	TM	TE,TM	
H_z	TE		TE	TE

In the above equations, k_r is the radial wavenumber, J_0 and J_1 are Bessel functions of order 0 and 1, respectively, and the integrations are over all possible wavenumbers k_r. The functions $g^{\mathrm{TE}}(p_{zI})$ and $g^{\mathrm{TM}}(p_{zII})$, which are functions of k_r, contain information about the seabed resistivity structure in the form of the generalized transverse electric (TE) and transverse magnetic (TM) reflection coefficients of a stack of conducting layers, including the air, sea and seafloor sediments. Full expressions for these functions can be found in Løseth & Ursin (2007) or derived in a slightly different form in Chew (1995).

For the case of TIV anisotropy, from eqs (119) in Løseth & Ursin (2007), it can be shown that within a given layer

$$p_{zI}^2 = \mu\tilde{\varepsilon}_h - \frac{k_r^2}{\omega^2}, \tag{5}$$

$$p_{zII}^2 = \mu\tilde{\varepsilon}_h - \frac{\tilde{\varepsilon}_h}{\tilde{\varepsilon}_v}\frac{k_r^2}{\omega^2}, \tag{6}$$

where $\tilde{\varepsilon} = \varepsilon + \frac{\mathrm{i}\sigma}{\omega}$ is the complex permittivity with the corresponding conductivity σ_h or σ_v for the horizontal or vertical directions within the layer. The terms ε and μ are the permittivity and permeability of free space, respectively. The term p_{zI} is the vertical 'slowness' (vertical wavenumber divided by the angular frequency ω) associated purely with the TE mode while the term p_{zII} is associated only with the TM mode. Thus, from eqs (5) and (6) it is apparent that the TE mode depends only on the horizontal conductivity while the TM mode depends on both the horizontal and vertical conductivity (e.g. Ramananjaona *et al.* 2011); this is expected given that the TE mode in 1-D layered structures is associated only with horizontal currents while the TM mode is associated with both horizontal and vertical currents.

The complete suite of fundamental dipole sources also includes the vertical electric dipole (VED), the horizontal magnetic dipole (HMD) and the vertical magnetic dipole (VMD). Each source produces particular modes in the EM field components, as listed in Table 1. The specific integral expressions for each field component and source type can be found in Løseth & Ursin (2007). For both the HED and HMD, the expressions for the radial electric field E_r, azimuthal electric field E_β, the radial magnetic field H_r and the azimuthal magnetic field H_β are mixtures of TE and TM modes, thus they contain sensitivity to both the horizontal and vertical conductivity of the seabed. Similarly, the three field components produced by a VED are entirely TM mode fields, which eq. (6) shows to contain sensitivity to the conductivity anisotropy. Conversely, the E_β, H_r and H_z components produced by a VMD are only TE mode fields and therefore are only sensitive to horizontal conductivity. Similarly, the H_z produced from either a HED or HMD is TE mode only and hence it is completely blind to the vertical conductivity.

While our understanding of the CSEM sensitivity to anisotropy is aided by knowledge of the modes present in each component, this knowledge does not address how well each component can resolve anisotropic conductivity. In an earlier study for isotropic conductivity, smooth inversions of synthetic data from each field component were used to identify which components can best recover a thin resistive layer representing a hydrocarbon reservoir, finding the HED transmitter to be overall superior for recovering the resistive layer as compared to the VED (Key 2009). While the smooth inversions were adequate for this purpose, they only produce a single conductivity model and offer no insights on the full range of models that might fit a given data set. Later in this work, we expand on this study by carrying out a Bayesian uncertainty analysis to characterize the resolution possible with each field component and also extend the model to include a modest amount of anisotropy in the overburden.

While either of the HED and HMD sources might be best for resolving anisotropy since they have the richest combination of modes, for practical reasons most marine CSEM surveys use a HED source. Very long HED antennas (100–500 m) can be deep-towed just above the seabed, creating a large source dipole moment that offers good signal-to-noise ratio data to long source–receiver offsets, whereas practically achievable HMD dipole moments result in much lower amplitude electric and magnetic fields and hence lower signal-to-noise ratios and a more limited range of usable source–receiver offsets. Hence the resolution study we present will focus only on the HED source.

2.2 Bayesian inversion

In the most general sense, the goal of geophysical studies is to provide information about the subsurface geology. Since Bayesian probability is a statement of information (e.g. Scales & Snieder 1997), a Bayesian framework for geophysical inversion seems natural to postulate.

We begin with Bayes' Theorem,

$$p(\mathbf{m}|\mathbf{d}) = \frac{p(\mathbf{d}|\mathbf{m})p(\mathbf{m})}{p(\mathbf{d})}, \tag{7}$$

where $\mathbf{d}$ is the vector of observed data and $\mathbf{m}$ is a vector of model parameters. However, in a Bayesian approach, all information is contained in PDFs represented by the notation $p(.)$. The idea is to estimate the posterior model distribution $p(\mathbf{m}|\mathbf{d})$ (i.e. the probability of the model given the data) starting from the knowledge of a prior model distribution $p(\mathbf{m})$ given the observed data $\mathbf{d}$. The information contained in the data is inserted into Bayes' theorem using the likelihood function $p(\mathbf{d}|\mathbf{m})$ which is the probability of the data given the model, (essentially the PDF of the data misfit as a function of $\mathbf{m}$). Assuming the noise in the data is Gaussian, we have the following likelihood function

$$p(\mathbf{d}|\mathbf{m}) \propto \exp\left(- \frac{[\mathbf{d} - f(\mathbf{m})]^T \mathbf{C_d}^{-1} [\mathbf{d} - f(\mathbf{m})]}{2} \right), \tag{8}$$

where $f(\mathbf{m})$ is the predicted data due to model $\mathbf{m}$ and $\mathbf{C_d}$ is the data covariance matrix, assumed here to be a diagonal matrix of data noise variances. The likelihood function in eq. (8) is formulated such that models with lower misfit demand a higher likelihood while poorly fitting models have less likelihood.

The evidence term $p(\mathbf{d})$ is equal to an integration of the numerator in the RHS of (7) over all possible models, and is therefore only a normalizing constant to ensure that $p(\mathbf{m}|\mathbf{d})$ integrates to 1; consequently it can be ignored, providing the following relationship

$$p(\mathbf{m}|\mathbf{d}) \propto p(\mathbf{d}|\mathbf{m})p(\mathbf{m}). \tag{9}$$

Thus it is now a matter of sampling the right hand side of eq. (9) to obtain the solution to the inverse problem and obtain the posterior model distribution. However, it is not possible to exhaustively sample the model space for more than a few parameters, hence in practice one resorts to efficient sampling methods like the Markov chain Monte Carlo (MCMC) method (e.g. Liang *et al.* 2010).

2.3 Reversible Jump MCMC

The RJ-MCMC is a particular type of Metropolis-Hastings (MH) algorithm (e.g. Liang *et al.* 2010) that allows one to search the model space such that models are not restricted in the number of parameters they may posses. Thus, they are said to be 'trans-dimensional' in the number of model parameters. In the context of the CSEM problem, the number of resistivity contrasts in the seabed is usually unknown *a priori* and should also be considered a part of the inverse problem. Malinverno (2002) considered this aspect of 'model selection' for the DC resistivity problem and Minsley (2011) applied this idea to the airborne frequency-domain EM problem. Formulating the inverse problem in a trans-dimensional manner allows for a broader characterization of the posterior model distribution, as demonstrated by Dettmer *et al.* (2010) for the geo-acoustic problem and Bodin & Sambridge (2009) for seismic tomography. There is a natural 'parsimony' (Malinverno 2002) built into the Bayesian RJ-MCMC framework. Simple models that fit the data well by using a few parameters are favoured over models with a larger number of parameters; this aspect of the RJ-MCMC Bayesian approach is similar to Occam's inversion, in which a penalty against model roughness is used to find a smooth model that only contains features required to fit the data (Constable *et al.* 1987). However, the trans-dimensional algorithm does not require any regularization or smoothing parameters, which are usually subjective choices for gradient based inversion methods. In short, a Bayesian RJ-MCMC framework is a truly data driven inversion scheme that parametrizes itself as demanded by the data.

The remainder of this section describes the details of the RJ-MCMC approach for the interested reader, but one could without loss of continuity skip to the example applications given in Section 3.

2.4 Prior information and model parametrization

In a pure Bayesian framework, prior information encapsulates knowledge about the model which is independent of the data. To be as general as is physically feasible, we use bounded uniform priors for all the model parameters of interest. In this section we closely follow the prior parametrization approach of Bodin & Sambridge (2009) but use interfaces (Dettmer *et al.* 2010) instead of Voronoi cells. We parametrize each model $\mathbf{m}$ as having n interfaces at depths z, and therefore $n + 1$ resistivities each for the horizontal resistivity ρ_h and for the vertical resistivity ρ_v, where resistivity $\rho = \sigma^{-1}$. The number of layers is fixed for a given model $\mathbf{m}$, hence

$$p(\mathbf{m}) = p(\mathbf{m}|n)p(n). \tag{10}$$

We use a uniform prior on n, given by

$$p(n) = \begin{cases} \frac{1}{n_{\max} - n_{\min}} & \text{if } n_{\min} \leq n \leq n_{\max} \\ 0 & \text{else} \end{cases}. \tag{11}$$

We assume no *a priori* knowledge between the depth of interfaces in the model and the layer resistivities (also considered independent), therefore their PDFs can be separated in the following product form,

$$p(\mathbf{m}|n) = p(\mathbf{z}|n)p(\rho_h|n)p(\rho_v|n). \tag{12}$$

Assuming interfaces can be located anywhere in the subsurface between $z_{\max}$ and $z_{\min}$ such that an interface can be at any of N (temporarily discrete) depths, for n interfaces, we can arrange them without paying attention to their ordering in $\frac{N!}{n!(N-n)!}$ ways. Note that this unspecified variable N will cancel out of the expressions we need to use in the algorithm and is only introduced for ease of mathematical derivation. Thus,

$$p(\mathbf{z}|n) = \begin{cases} \left[\frac{N!}{n!(N-n)!}\right]^{-1} & \text{if } z_{\min} \leq z \leq z_{\max} \\ 0 & \text{else} \end{cases}. \tag{13}$$

Assuming that all $n+1$ resistivities, ρ_h and ρ_v lie uniformly between $\rho_{\min}$ and $\rho_{\max}$, independent of each other, we write

$$p(\rho_h|n)p(\rho_v|n) = \begin{cases} \left[\frac{1}{\rho_{\max}-\rho_{\min}}\right]^{2(n+1)} & \text{if } \rho_{\min} \leq \rho \leq \rho_{\max} \\ 0 & \text{else} \end{cases}. \tag{14}$$

To obtain the explicit expression for the prior model probability, we write $\Delta\rho = \rho_{\max} - \rho_{\min}$ and $\Delta n = n_{\max} - n_{\min}$ and substitute eqs (11)–(14) into (10) to get

$$p(\mathbf{m}) = \begin{cases} \frac{n!(N-n)!}{N!\Delta n(\Delta\rho)^{2n+2}} & \text{if } z \in [z_{\min}, z_{\max}] \text{ and } \rho \in [\rho_{\min}, \rho_{\max}],\ \forall n \in [n_{\min}, n_{\max}] \\ 0 & \text{else} \end{cases}. \tag{15}$$

2.5 MH algorithms and the acceptance probability

What guides an MCMC sampler like the MH algorithm to convergence upon the posterior distribution is the acceptance probability α (e.g. Liang *et al.* 2010). At every step of the Markov Chain, a candidate model is sampled by perturbing the current model from a known distribution (the proposal distribution q) and the acceptance α is calculated. A random number r is then sampled uniformly from the interval [0,1]. If $r < \alpha$ the proposed perturbation is accepted, else the old model is retained. The rationale behind this algorithm can be explained by examining in more detail the expression for α (Bodin & Sambridge 2009), where

$$\alpha(\mathbf{m}'|\mathbf{m}) = \min\left[1, \frac{p(\mathbf{m}')}{p(\mathbf{m})} \times \frac{p(\mathbf{d}|\mathbf{m}')}{p(\mathbf{d}|\mathbf{m})} \times \frac{q(\mathbf{m}|\mathbf{m}')}{q(\mathbf{m}'|\mathbf{m})} \times |\mathbf{J}|\right]. \tag{16}$$

Here $\mathbf{m}'$ is the new proposed model and $\mathbf{m}$ is the old model (throughout this paper, primes will denote new model values). Specifically, $\frac{p(\mathbf{m}')}{p(\mathbf{m})}$ is the prior ratio, $\frac{p(\mathbf{d}|\mathbf{m}')}{p(\mathbf{d}|\mathbf{m})}$ is the likelihood ratio and $\frac{q(\mathbf{m}|\mathbf{m}')}{q(\mathbf{m}'|\mathbf{m})}$ is the proposal ratio. The Jacobian term $|\mathbf{J}|$ is not to be confused with the model Jacobian needed for gradient based inversions (e.g. Constable *et al.* 1987), but is a matrix that incorporates changes in model dimension when moving from $\mathbf{m}$ to $\mathbf{m}'$. In a classic MH algorithm with a fixed number of dimensions, the prior ratio, proposal ratio (for symmetric proposals), and Jacobian term are all 1 (Dettmer *et al.* 2010). Hence the algorithm always moves towards areas of higher posterior probability if the data misfit improves (likelihood ratio >1). However, it can also move to areas of lower posterior probability with a probability α if the misfit does not improve (likelihood ratio <1).

To be able to compare likelihoods between models with different numbers of parameters (i.e. with different dimensions), the Jacobian in the acceptance term in eq. (16) needs to be evaluated. There are various implementations of RJ-MCMC, and in all the examples cited so far, a 'birth–death' scheme has been used. As shown in Bodin & Sambridge (2009) and Dettmer *et al.* (2010) for the 'birth–death' RJ-MCMC scheme, this Jacobian term is unity. We have adopted the 'birth–death' algorithm in this paper and shall not concern ourselves with this Jacobian term any further.

As to why the algorithm should not always look to improve the data fit by simply increasing the number of parameters (interfaces in the seabed), if we examine eq. (16) we find that even if the likelihood ratio times the proposal ratio is greater than one for a proposed move that inserts a new interface into the model, the prior ratio will be less than one owing to the fact that the new prior PDF $p(\mathbf{m}')$ needs to integrate over a larger number of parameters to equal 1. Hence, there is an opposition to the 'birth' of a new layer (which may lead to improvement of data fit) by the prior ratio.

2.6 Outline of our algorithm

We start the algorithm with a 'minimum structure model', following the approach of Agostinetti & Malinverno (2010). Placing one layer above a halfspace (i.e. $n = 1$) we start with a single interface and then allow the algorithm to iteratively add interfaces ('birth') or remove them ('death'), perturbing the layer resistivities, as the data may demand via the acceptance probability α in (16).

We then closely follow the 'partition modelling' approach of Bodin & Sambridge (2009), but use layer interfaces instead of their Voronoi cells (Dettmer *et al.* 2010). We perturb candidate model resistivities just as Agostinetti & Malinverno (2010) perturb elastic properties for their seismic receiver function problem. We depart from the above methods in our implementation by randomly using a local (small) or

global (large) proposal for perturbing resistivities when the number of dimensions is fixed (i.e. it is not a birth or death move) as suggested in Andriéu *et al.* (2003). In brief, this is how we proceed:

2.6.1 Initialization

Start the algorithm with $n = 1$ and layer resistivities sampled randomly from the uniform prior distribution represented by eq. (14).

2.6.2 Update layer properties

At every even numbered step we perturb *all* the $2(n + 1)$ layer resistivities about their current values using a Gaussian proposal $q(\mathbf{m}'|\mathbf{m})$ with a standard deviation Σ_ρ, where

$$q(\mathbf{m}'|\mathbf{m}) = \left(\frac{1}{\sqrt{2\pi}\,\Sigma_\rho}\right)^{2n+2} \exp\left[-\frac{1}{2\Sigma_\rho^2}(\rho' - \rho)^T(\rho' - \rho)\right]. \tag{17}$$

Note that this update move does not involve a change in the number of interfaces.

It is in this move that we depart from previously carried out work, by randomly switching between an update proposal step size of Σ_ρ to a smaller step size $f\Sigma_\rho$. f is a fraction to be determined by the problem at hand and is constant throughout the algorithm. The randomly selected step size allows the algorithm to take global or local steps while sampling the model space during fixed dimension moves (Andriéu *et al.* 2003).

2.6.3 Perturb model geometry

At every odd numbered step we allow one of the following 4 moves:

(1) Birth of an interface: $n' = n + 1$. Uniformly between $z_{\min}$ and $z_{\max}$, we randomly select an unoccupied depth and insert an interface. The layer above or below the newly created interface is randomly selected and only its horizontal and vertical resistivity are perturbed according to a 2-D Gaussian proposal with standard deviation Σ'_ρ.

(2) Death of an interface: $n' = n - 1$. An existing interface is selected at random and deleted. The new horizontal and vertical resistivity in the layer are randomly copied from one of the two layers that used to exist on either side of the deleted interface.

(3) Move an interface: $n' = n$. An existing interface is selected at random and its depth perturbed by a 1-D Gaussian proposal with standard deviation Σ_m. If the new interface depth is shallower or deeper than the interfaces currently above or below it, this move can be thought of as a simultaneous death/birth move, that is, properties from one of the layers on either side of the old interface are copied (at random) and assigned to one of the layers on either side of the new interface position (also at random).

(4) No perturbation: $n' = n$ and $\mathbf{z}' = \mathbf{z}$.

Each of these model geometry perturbation moves is applied with a certain probability, such that their sum equals 1. In addition, the birth and death probabilities are set equal. We set the probabilities as follows: [birth, death, move, no perturbation] $\equiv \left[\frac{3}{8}, \frac{3}{8}, \frac{1}{8}, \frac{1}{8}\right]$.

At each step of the Markov chain, the proposed model is evaluated for acceptance. If it is accepted, it becomes the current model. If it is rejected, the current model is preserved and the algorithm moves on to the next step. To compute the acceptance, one needs to evaluate eq. (16), for which we explicitly describe the proposal distributions and their ratios in the next section.

2.7 Proposal distributions and acceptance probabilities

Our proposal distributions are similar to those described in Bodin & Sambridge (2009) and Dettmer *et al.* (2010), but since the trans-dimensional approach to the best of our knowledge has not been used for solving the CSEM problem we review the model proposals in modest detail here.

2.7.1 Fixed dimension moves

For all moves that are neither birth nor death, the number of interfaces remain fixed. In these moves, we have elected to use Gaussian proposals to suggest the new model parameters by centring the proposals on the old parameters and drawing a random number from a normal distribution with a given standard deviation (step size). As can be seen from eq. (17) these kinds of moves are symmetric, implying that the probability to go from the old state to the new state is the same as it would be in going from the new state to the old state

$$\left[\frac{q(\mathbf{m}|\mathbf{m}')}{q(\mathbf{m}'|\mathbf{m})}\right]_{\text{fixed}} = 1. \tag{18}$$

Since the number of dimensions remains constant, the prior ratio in eq. (16) is 1. Hence for fixed dimension moves, we find that the acceptance probability is simply the ratio of the likelihoods:

$$\alpha_{\rm f} = \begin{cases} \min\left[1, \frac{p(\mathbf{d}|\mathbf{m}')}{p(\mathbf{d}|\mathbf{m})}\right] & \text{if } z \in [z_{\min}, z_{\max}] \text{ and } \rho \in [\rho_{\min}, \rho_{\max}],\ \forall n \in [n_{\min}, n_{\max}] \\ 0 & \text{else} \end{cases}. \tag{19}$$

2.7.2 Birth move

For a birth move, one can select from out of $N - n$ unoccupied spaces. The perturbations for the birthed layer's horizontal and vertical resistivity are drawn from a 2-D Gaussian with standard deviation Σ_{bd}, centred about the old values in the layer. Since the selection of an interface depth and the perturbations are independent, we can write

$$q(\mathbf{m}'|\mathbf{m}) = q(\mathbf{z}'|\mathbf{m})\, q(\rho'|\mathbf{m}) \tag{20}$$

$$= \frac{1}{(N-n)} \frac{1}{2\pi\, \Sigma_{bd}^2} \exp\left[- \frac{(\rho_h' - \rho_h)^2 + (\rho_v' - \rho_v)^2}{2\Sigma_{bd}^2} \right]. \tag{21}$$

For the reverse move in a birth, keeping in mind that the current state has n interfaces, a birth would have $n + 1$ interfaces to delete from, and the probability of removing resistivities in a layer in the reverse move is 1, thus we can say that

$$q(\mathbf{m}|\mathbf{m}') = q(\mathbf{z}|\mathbf{m}')\, q(\rho|\mathbf{m}') \tag{22}$$

$$= \frac{1}{(n+1)} \times 1. \tag{23}$$

Thus in a birth move, from eqs (21) and (23), the proposal ratio can be written as

$$\left[\frac{q(\mathbf{m}|\mathbf{m}')}{q(\mathbf{m}'|\mathbf{m})}\right]_{\rm birth} = \frac{(N-n)2\pi\, \Sigma_{bd}^2}{n+1} \exp\left[\frac{(\rho_h' - \rho_h)^2 + (\rho_v' - \rho_v)^2}{2\Sigma_{bd}^2} \right]. \tag{24}$$

Finally from eqs (15), (16) and (24) we get for the birth moves, the following acceptance probability

$$\alpha_{\rm b} = \begin{cases} \min\left[1, \frac{2\pi\, \Sigma_{bd}^2}{\Delta\rho^2} \exp\left[\frac{(\rho_h' - \rho_h)^2 + (\rho_v' - \rho_v)^2}{2\Sigma_{bd}^2}\right] \frac{p(\mathbf{d}|\mathbf{m}')}{p(\mathbf{d}|\mathbf{m})}\right] & \text{if } z \in [z_{\min}, z_{\max}],\ \rho \in [\rho_{\min}, \rho_{\max}],\ \forall n \in [n_{\min}, n_{\max}] \\ 0 & \text{else} \end{cases}. \tag{25}$$

2.7.3 Death move

In a death move, one can select one of n places for deletion. Further, the probability of removing resistivities in a layer is certain. Thus,

$$q(\mathbf{m}'|\mathbf{m}) = q(\mathbf{z}'|\mathbf{m})\, q(\rho'|\mathbf{m}) \tag{26}$$

$$= \frac{1}{n} \times 1. \tag{27}$$

In the reverse move for death, since the reference state has n interfaces, there are $N - (n - 1)$ sites at which to add an interface. Further, the resistivity perturbations are proposed using a 2-D Gaussian centred around the current values. Hence

$$q(\mathbf{m}|\mathbf{m}') = q(\mathbf{z}|\mathbf{m}')\, q(\rho|\mathbf{m}') \tag{28}$$

$$= \frac{1}{N-n+1} \times \frac{1}{2\pi\, \Sigma_{bd}^2} \exp\left[- \frac{(\rho_h - \rho_h')^2 + (\rho_v - \rho_v')^2}{2\Sigma_{bd}^2} \right]. \tag{29}$$

Thus we can see from eqs (27) and (29) that the proposal ratio for death can be written as

$$\left[\frac{q(\mathbf{m}|\mathbf{m}')}{q(\mathbf{m}'|\mathbf{m})}\right]_{\rm death} = \frac{n}{(N-n+1)2\pi\, \Sigma_{bd}^2} \exp\left[- \frac{(\rho_h - \rho_h')^2 + (\rho_v - \rho_v')^2}{2\Sigma_{bd}^2} \right]. \tag{30}$$

Again from eqs (15), (16) and (30) we get for the death moves, the following acceptance probability

$$\alpha_{\rm d} = \begin{cases} \min\left[1, \frac{\Delta\rho^2}{2\pi\Sigma_{bd}^2}\exp\left[-\frac{(\rho_h'-\rho_h)^2+(\rho_v'-\rho_v)^2}{2\Sigma_{bd}^2}\right]\frac{p(\mathbf{d}|\mathbf{m}')}{p(\mathbf{d}|\mathbf{m})}\right] & \text{if } z \in [z_{\min}, z_{\max}],\ \rho \in [\rho_{\min}, \rho_{\max}],\ \forall n \in [n_{\min}, n_{\max}] \\ 0 & \text{else} \end{cases}. \quad (31)$$

It should be noted that the derived expressions for α in eqs (19), (25) and (31) do not involve the variable N (as promised) and are very similar in form to the expressions derived in Bodin & Sambridge (2009). This demonstrates how flexible the algorithm is when solving completely different kinds of geophysical problems.

2.8 Convergence to the posterior distribution

The algorithm is run for a given number of steps until it is deemed to have collected enough samples to provide a reasonable estimate of the posterior. There are a couple of caveats in this regard, as there are with any MCMC sampler (Liang *et al.* 2010). If the algorithm is seeded with an initial model that is in a low posterior probability region, it may take quite a few steps till it reaches a region of high posterior probability, such that it begins to sample models which fit the data within the given data error. The number of such required steps (which are subsequently discarded in the final chain) is known in MCMC parlance as the 'burn-in' period, which depends on how well the proposal distributions have been scaled (Chib & Greenberg 1995). This brings us to the step sizes (scaling) in the proposal distributions in the form of the standard deviations Σ_ρ, Σ_m, Σ_{bd} and the fraction f required in the various proposals to generate a new candidate model. The form of the proposal distributions should 'emulate' the posterior for efficient sampling, but since the posterior distribution may be complicated (and unknown *a priori*), any kind of simple distribution, symmetric where possible, can be used. The exact form of the proposal does not affect convergence. The suitability of the step size for the problem at hand can be examined by looking at the number of samples accepted in a large interval of steps, referred to as the acceptance rate. If the acceptance rate is too low, it means that the step sizes are too large as lots of steps are falling outside the prior bounds or are being rejected as they land in low probability (high misfit) areas. If the acceptance rate is too high, then it implies that the algorithm isn't exploring the model space enough and will again be slow to converge upon the posterior distribution. While the sampled posterior should not depend on the size of the steps taken, one has to factor in the optimality of the step size as otherwise convergence will be very slow (Bodin & Sambridge 2009). For an illuminating discussion on this matter, one can refer to Chib & Greenberg (1995) or Trainor-Guitton & Hoversten (2011) for a more recent discussion relevant to marine CSEM. For further discussions on convergence diagnostics and the practicality of their application, one can refer to Liang *et al.* (2010) The algorithm should be run long enough at the lowest acceptable rms (achieved after the burn-in period) such that there is at least stationarity achieved in the square misfit with iteration number. Further, to ensure that the inferred posterior is not biased due to being trapped in local maxima (of the posterior probability), we recommend that the algorithm be run from many different starting points, ideally in parallel for computational efficiency. The final ensemble for posterior inference can be constructed by concatenating the various parallel chains (e.g. Agostinetti & Malinverno 2010; Dettmer *et al.* 2010; Bodin *et al.* 2012).

2.9 Implementation details

We implemented the trans-dimensional Bayesian inversion algorithm in MATLAB since it allowed for rapid prototyping, testing and modification. Specifically, we coded the comprehensive suite of equations for magnetic and electric dipole sources embedded in TIV anisotropic media that are listed in appendix F of Løseth & Ursin (2007). The Hankel transform integrals are evaluated using the digital filters and lagged convolution MATLAB codes that are freely available in Key (2012a). To speed up the program's performance, the portion handling the 1-D CSEM forward calls was converted to C and precompiled as a MEX (MATLAB Executable) using the MATLAB Coder utility. The numerical CSEM responses from the forward code were validated by comparisons with suites of anisotropic responses given in Løseth & Ursin (2007) and Li & Dai (2011). We validated the reliable sampling of the trans-dimensional Bayesian algorithm by ensuring that we could sample and recover the specified uniform prior model distribution by removing the data and running the RJ-MCMC algorithm. Since resistivity can span many orders of magnitude, we follow the usual approach for EM geophysics and parametrized the code to invert for $\log_{10}$(resistivity) rather than its linear counterpart.

3 EXAMPLE APPLICATIONS

3.1 Synthetic studies for the resolution of a thin resistive layer

In this example application, we use the trans-dimensional inversion algorithm to study how well each CSEM field component can resolve the anisotropic resistivity of an offshore hydrocarbon reservoir model. In a previous study conducted for a simple isotropic reservoir model, the Occam inversion method was used to find the smoothest inversion model for each data component, generally showing that the field

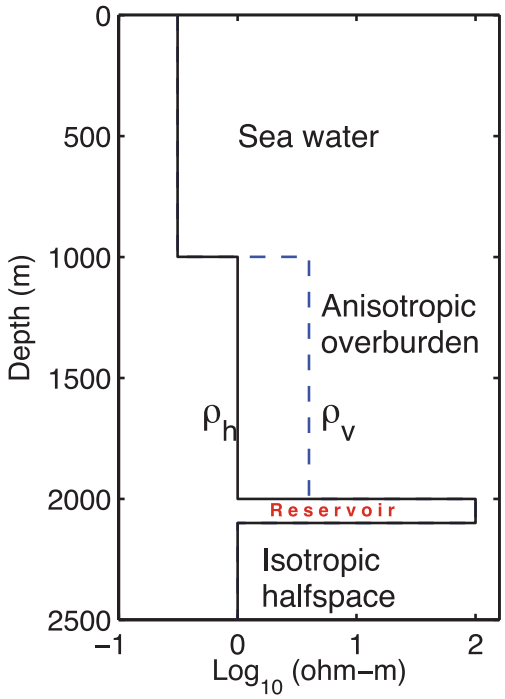

Figure 1. Synthetic model of a thin resistive hydrocarbon reservoir with overlying anisotropic conductive sediments. The horizontal resistivity is shown in solid black, and the vertical resistivity with blue dashes.

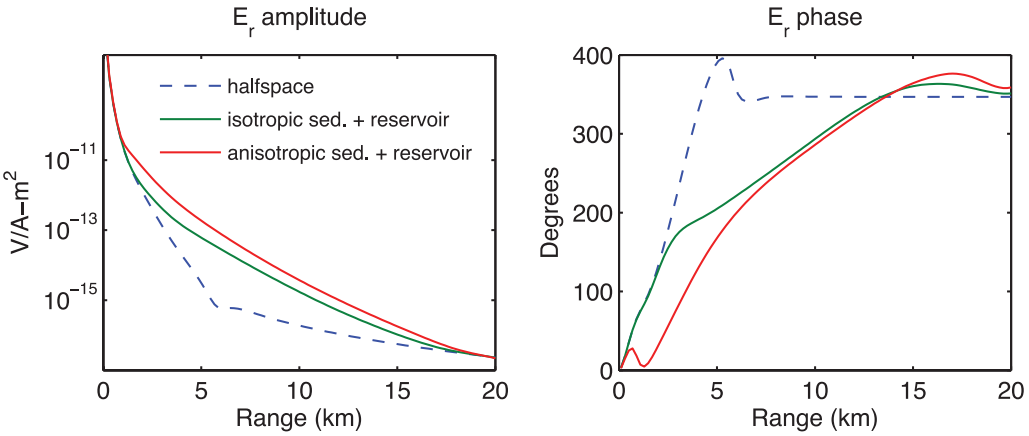

Figure 2. Source normalized CSEM responses shown as magnitude versus offset (MVO) and phase versus offset (PVO) curves for the radial electric field at 0.7 Hz produced by a horizontal electric dipole (HED). Plotted responses correspond to an isotropic 1 ohm-m seafloor in 1 km of water (dashed blue), the isotropic model corresponding only to ρ_h in Fig. 1 (green) and the full anisotropic model in Fig. 1 (red).

components from a HED are best able to recover the sediment and reservoir resistivity as compared to a VED (Key 2009). In addition, because the HED data are the most commonly collected on commercial surveys, we restrict our synthetic studies here to data generated from a HED.

The model under consideration is based on the well-studied canonical 1-D reservoir model (e.g. Constable & Weiss 2006) but here has been updated to include a moderate amount of anisotropy in the overburden sediments, as shown in Fig. 1. The main feature of the model is a 100 m thick, 100 ohm-m isotropic reservoir located 1 km beneath the seafloor. The overburden resistivity is 1 ohm-m in the horizontal direction but 4 ohm-m in the vertical direction, representative of bulk anisotropy due to sediment layering.

We modelled 20 source–receiver offsets spaced evenly from 0 to 12 km, with the transmitter positioned 10 m above the seafloor and broadcasting frequencies 0.1, 0.3 and 0.7 Hz. As an example of the contributions of the various model features to the CSEM responses, Fig. 2 shows the inline radial electric field E_r magnitude versus offset (MVO) and phase versus offset (PVO) responses for the anisotropic model (red), a similar model but where the sediments are isotropic with 1 ohm-m resistivity (green), and a model with a uniform 1 ohm-m isotropic sediments (dashed blue). The resistive reservoir can be seen to be the largest contributor to the responses, but the overburden anisotropy also contributes substantially to the increased MVO responses accompanied by markedly different PVO responses.

Synthetic data were generated for both inline and broadside transmitter geometries by adding 5 per cent random Gaussian noise to the model responses and then removing data below amplitudes of 10^{-15} V A^{-1}m^{-2} for electric fields and 10^{-18} T A^{-1}m^{-1} for magnetic fields, representative of the electric and magnetic field noise floors for currently available CSEM transmitter–receiver systems with 60 s data stacks.

The trans-dimensional algorithm was independently applied to the synthetic noisy data for each of the 6 EM field components to obtain the marginal PDFs on the model parameters, which then can be used to compare the resolution properties of each component. We allowed the number of interfaces to range from 1 to 30, and the range of depths at which to place interfaces from 1005 to 2500 m. We used uniform prior distributions on the log-resistivities in the seafloor that allowed them to vary between -1 and 2.3 (corresponding to linear resistivities of 0.1 to 200 ohm-m). For each field component, a total of 200 MCMC chains were run in parallel (each starting point was randomly sampled from the prior distribution), with 2 million steps taken in each each chain. Approximately 1/3 of the chain length was discarded as part of the initial 'burn-in' process (Dettmer *et al.* 2010) and the remaining steps were collected. The length of the 'burn-in' period was determined by monitoring for when the algorithm reached an rms data misfit value of $\approx$1 (corresponding to a χ^2 value equal to the number of data points); after the burn-in period, the algorithm continued to sample models that fit the data within an acceptable data rms misfit. The final concatenated MCMC chain is constructed from all 200 parallel runs, but with care to only concatenate chains that have converged upon the region of acceptable rms. Those chains, which even after 'burn-in' failed to achieve an rms close to 1 were discarded (Trainor-Guitton & Hoversten 2011). For each field component's inversion, the final concatenated chains consists of roughly 200 000 models after thinning the chain to retain 1 out of every 1000 samples (as a means of reducing the storage requirements and the burden for later plotting algorithms). We found that a further decimation of 1 in every 4 models produced acceptable PDFs, with a final sample size of around 50 000 models. Since this trans-dimensional method has not been applied to marine CSEM data before (to the best of our knowledge), we preferred to be cautious rather than undersample the parameter PDFs. The implication is that we potentially could have used a smaller number of parallel MCMC chains or a shorter chain length, or some combination of both to significantly reduce the computational load of this task, given that we achieved acceptance rates between 12 and 22 per cent. These acceptance rates are in agreement with those reported by Dettmer *et al.* (2010) and Agostinetti & Malinverno (2010).

The final ensembles for each data component consist of about 50 000 1-D models, each of which contains a variable number of layers, the layer interface depths and the horizontal and vertical resistivities of each layer. To visualize the range of acceptable resistivities, we binned these parameters into a grid of fine depth intervals to produce a histogram of resistivities at each depth, normalized by the total number of resistivities encountered in a depth bin. Higher histogram values at a particular depth bin indicate a higher probability of the resistivity being at the corresponding value at that depth. Similarly, the probability that an interface exists at a certain depth is shown by binning the interface depths required by the various models over a range of fine depth intervals.

The results are shown in Fig. 3, where each row corresponds to an inversion of a certain EM field component. In every row, the first two columns correspond to PDFs of the horizontal and vertical resistivity as a function of depth, with the 5 per cent and 95 per cent quantiles at each depth shown in blue. The true model is shown in red, and higher values of probability at a depth are shown by darker shading. The third column in each row corresponds to the probability of a layer interface at a given depth, with the true values at which interfaces are located indicated by red horizontal lines. The fine black vertical line in this column corresponds to a uniform probability on the location of interfaces. Again, higher values indicate a greater probability for the presence of a resistivity contrast at the corresponding depth. Fig. 4 shows the probability of the number of interfaces required for each particular field component, where the vertical red line denotes the true value of two interfaces for our three layered anisotropic model.

From the synthetic inversions we can make a number of observations. The vertical resistivities for all components (with the exception of H_z which is a pure TE mode) have the most probable value aligned with the true value at shallower depths. At the reservoir and greater depths, the well-known trade-off between reservoir thickness and resistivity (Constable & Weiss 2006; Key 2012b) results in the PDFs being more diffuse, yet still concentrated near the true resistivity. Further, there is a marked increase in the 95 per cent quantile line in the vicinity of the reservoir whereas at much shallower depths the 95 per cent quantiles suggest there is little probability of a resistive layer.

For the horizontal resistivities, the most probable values at shallow depths are also closely aligned with the true value until the reservoir level, where there is an abrupt decrease as the PDF becomes greatly spread out with no significant peak and the confidence of the estimate (indicated by the width between the 5 and 95 per cent quantiles) at these depths is quite low. This inability to resolve the horizontal resistivity within the reservoir is not surprising, as the current density in the resistive reservoir layer becomes predominantly vertically polarized with little horizontal flow and hence contains greatly diminished sensitivity to the horizontal resistivity at this depth (Brown *et al.* 2012). There is however, a slight increase in the 95 per cent limit around the reservoir depth at least suggesting the probability of an increased resistivity at this depth. Perhaps surprisingly, the lower halfspace resistivities are well imaged by the horizontal resistivity PDFs, probably owing to the fact that to complete the circuit, current must flow horizontally at this depth.

The interface depth probabilities in Fig. 3 show that all components (with the exception of H_z) have a high probability for layer interfaces near the correct depths of the reservoir. Some estimate well either the reservoir top (by E_r) or the reservoir bottom (by H_β or H_r) or both the top and bottom (by E_β and E_z). The vertical magnetic field H_z seems unable to clearly estimate either the reservoir top or bottom, but this is unsurprising given that it only contains the TE mode which is well-known to be insensitive to thin resistive layers. The ability of the E_z to recover both the top and bottom depths of the reservoir is intriguing, particularly since previous smooth inversion studies suggested it has slightly lower resolution for the reservoir thickness (see fig. 7 in Key 2009). While all other components (besides H_z) contain a mixture of TE and TM modes, the E_z component only contains the TM mode; perhaps its ability to resolve the reservoir boundaries is due to galvanic charge accumulation effects. Further exploration of this result is clearly warranted but is beyond the scope of this work.

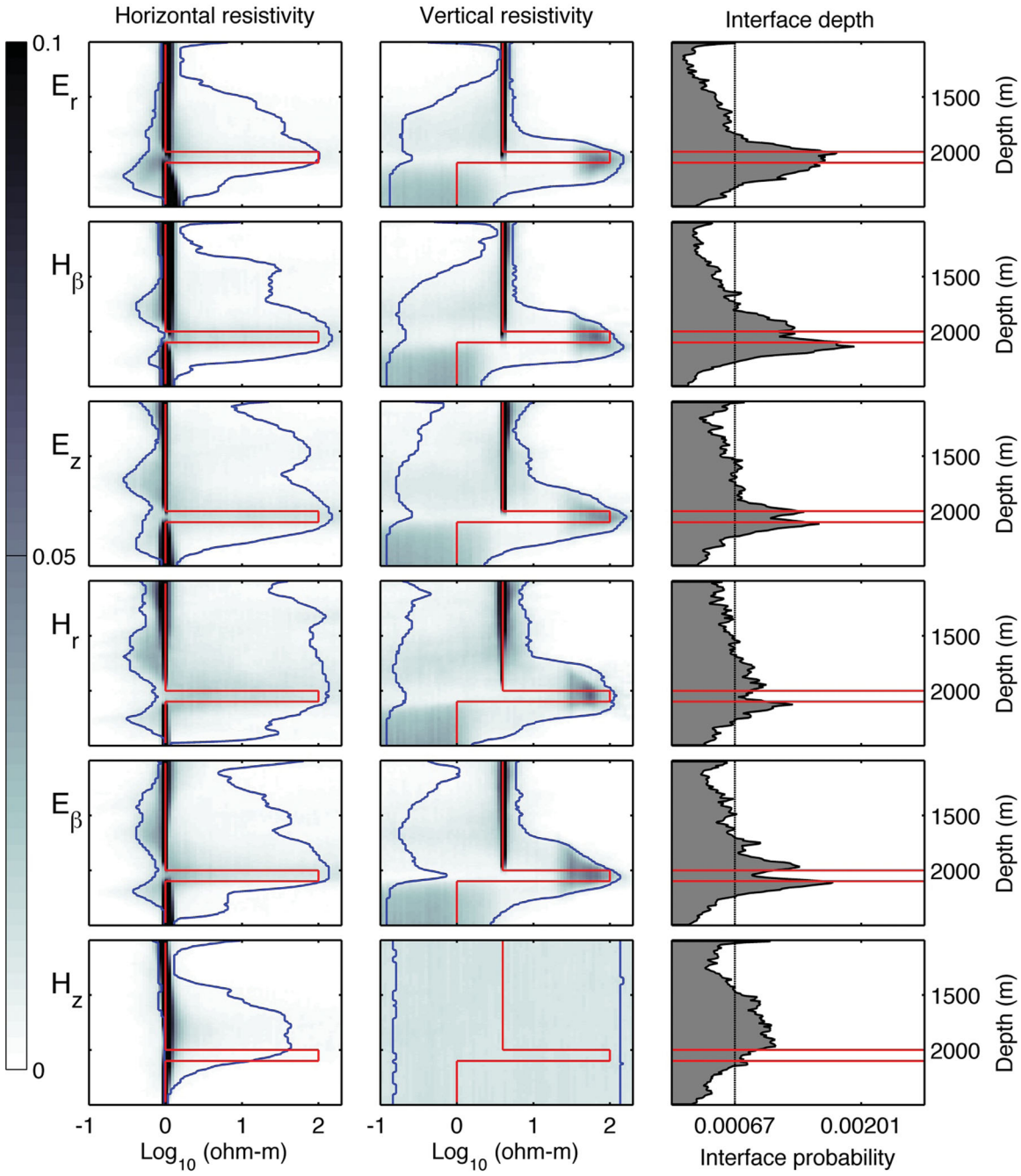

Figure 3. Trans-dimensional Bayesian inversion of synthetic HED data with 5 per cent added noise. The results from independent inversion of each field component are shown row wise. Marginal distributions on anisotropic resistivity values at depth are shown as shaded colours in the first two columns while the third column indicates the probability of an interface. 5 per cent and 95 per cent quantile lines are shown in blue and the true values are indicated by red lines. The top three rows correspond to the components measured by receivers inline with the HED while the bottom three rows are for components measured by receivers broadside to the HED.

Anisotropy in the shallower section is well resolved by all components (again with the exception of H_z), with the tightest bounds on anisotropy being given by the inline radial electric field. For all these components, a good indicator for the presence of a resistive reservoir seems to be the combination of the peak in the interface depth probabilities aligning with a high probability of large vertical resistivity. As can be seen in Fig. 3, this alignment occurs around the true reservoir vertical resistivity and depth.

The probability for the number of interfaces shown in Fig. 4 illustrates that the algorithm did not spend much time testing a large number of layers (which require longer times per forward call), suggesting a computational efficiency advantage to using the RJ-MCMC sampler over alternative approaches using a large number of fixed layer interfaces. In fact, one suggested approach when using this algorithm is to first look at the ensemble of all inverted models to identify the most probable number of layer interfaces, and then to examine the PDFs for the subset of models with that number of layers.

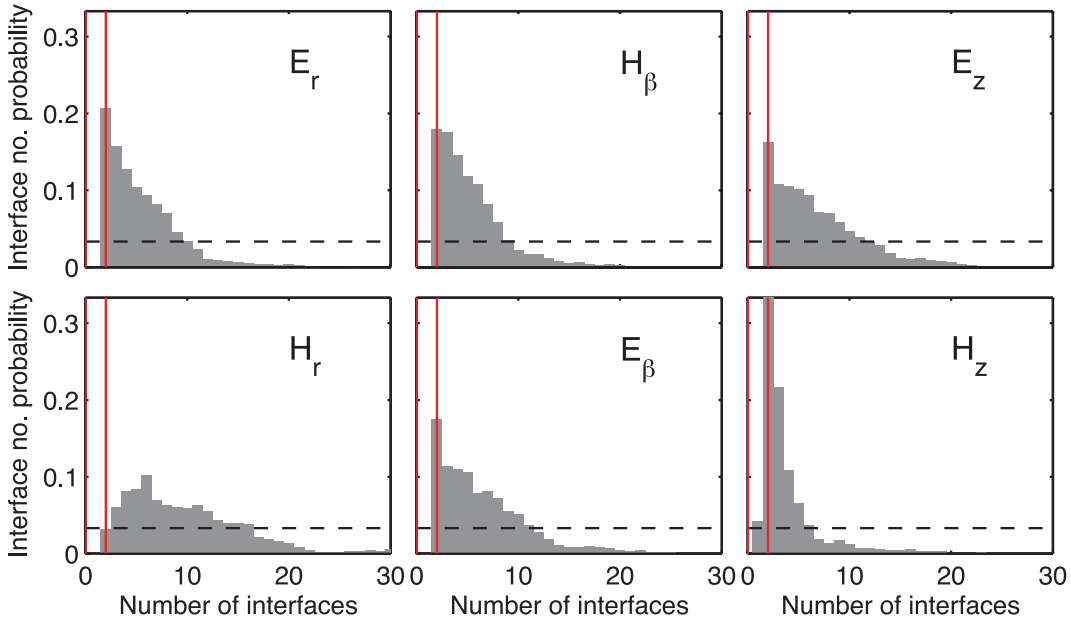

Figure 4. Probability of the number of interfaces determined from independent inversions of synthetic data for each field component. The true number of interfaces (2) is shown by the red line. The fine dashed black horizontal line corresponds to a uniform probability on the number of interfaces.

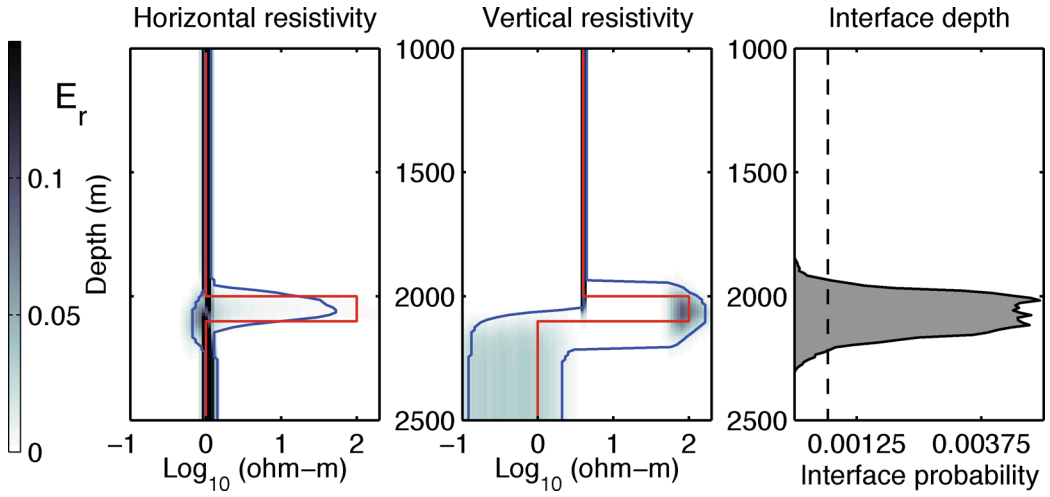

Figure 5. Subset of the posterior ensemble for the E_r synthetic data inversion where the number of interfaces is equal to the true value of 2. The 5 per cent and 95 per cent quantiles are far tighter than for the full ensemble shown in Fig. 3.

Fig. 5 shows that when we subset the posterior ensemble to display only models which require two interfaces (i.e. three layers) to fit the data, which of course is the true number of interfaces in the synthetic model, we get very tight constraints on the ensuing distributions for the radial inline electric field data. This agrees with a previous studying showing a tight region of low misfit in the two parameter model space of reservoir resistivity and thickness (Key 2012b). In an exploration scenario, the 'data mining' or post-processing of the trans-dimensional inversion results opens up the possibility of incorporating more information as and when it becomes available during the interpretation phase, in order to obtain more certainty in the inverted results without having to perform any further inversion—as the full posterior model solution only needs to be subsetted for this kind of exploration of model space. This ability is further explored in our application to real data, as described in the next section.

3.2 Application to data from the Pluto gas field, Northwest Shelf of Australia

In this section, we apply the trans-dimensional inversion to real CSEM survey data collected over the Pluto gas field on the Northwest Shelf of Australia as part of a commercial survey in early 2007. A previous analysis of this single site of CSEM data was presented in the context of solving for unknown receiver orientations in Key & Lockwood (2010). Pluto together with the close by Xena field comprise a five TCF gas accumulation (Tilbury *et al.* 2009). The discovery well Pluto-1 found a gas column of 209 m gross thickness approximately 3100 m below sea level in a sandy tilted Triassic fault block, with an average net porosity of 28 per cent with gas saturations in the main reservoir of around

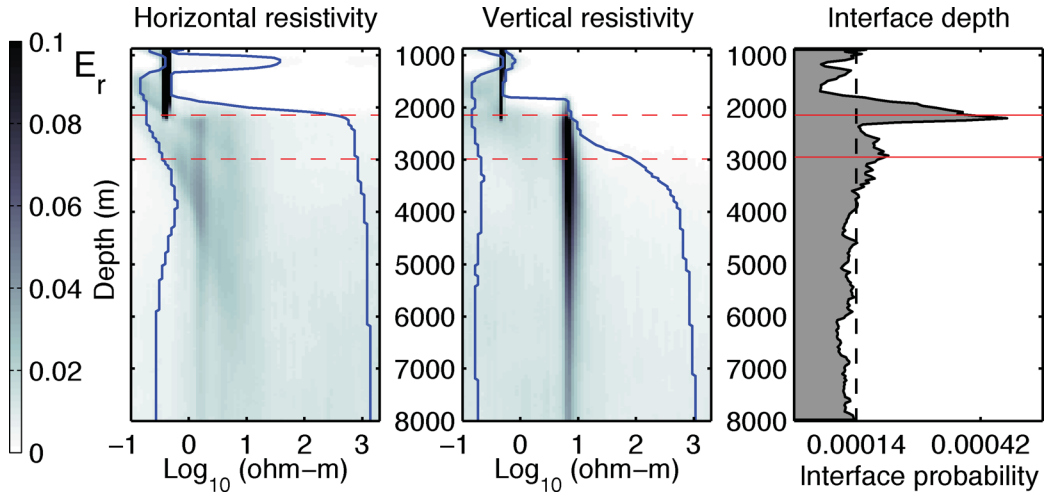

Figure 6. Results of the trans-dimensional inversion of the Pluto inline radial electric field data for a single receiver. Interfaces with high resistivity contrast are indicated and marked with red horizontal lines at 2150 m and 2950 m depth (right panel), with the values of most probable vertical resistivity at these depths being 10 ohm-m (middle panel). Note the similarities with the synthetic studies of E_r on encountering a resistor at depth—the horizontal resistivity PDFs become diffuse (left panel) but there is a pronounced peak in the vertical resistivity PDFs.

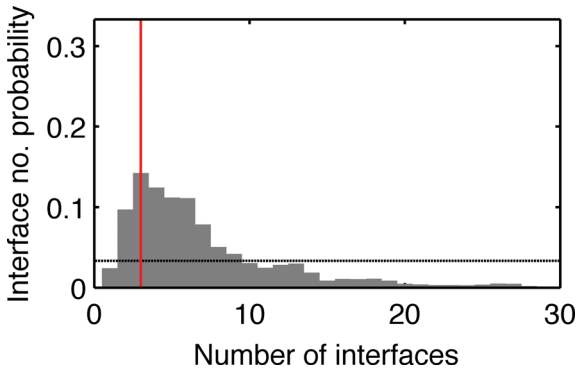

Figure 7. PDF of the number of interfaces required to fit the Pluto data. The most probable number of interfaces is three.

93 per cent. Radial inline electric field data collected at 0.24 and 0.4 Hz for a single site were inverted using the trans-dimensional RJ-MCMC method described in this paper.

The trans-dimensional inversion results for the resistivity PDFs and the number of interfaces required are shown in Figs 6 and 7, respectively. The horizontal and vertical resistivity as a function of depth shows little evidence of anisotropy from the seafloor down to 2000 m, with the most probable resistivity value being 0.5 ohm-m. However, the 5 per cent and 95 per cent quantile lines on the horizontal resistivity are larger than the very narrow PDFs of the vertical resistivity in this depth interval. The interface probability as a function of depth (third column in Fig. 6) suggests a large probability of an interface at 2150 m, followed by another peak at 2950 m. The vertical resistivity jumps to a most probable value around 10 ohm-m accompanied by an increase in the 95 per cent quantile on resistivities at depth. This is very similar to what we observed in our synthetic studies on E_r, as can be seen by comparing Fig. 3 with Fig. 6. Further, at depths beyond 2000 m the horizontal resistivity PDFs are very diffuse, again similar to what was seen in the synthetic studies in resistive layers. However, as there seem to multiple resistive targets at depths beyond 2000 m, the PDFs do not show a narrowing again as they they did for the single resistive layer synthetic data, but instead are more diffuse indicating that resolution decreases with depth, as expected for CSEM on the conductive sediments of the continental shelves. The most probable number of interfaces, from Fig. 7 is 3.

The data fit for 50 randomly sampled models (out of a total of 94 450) in the final posterior model distribution is shown in Fig. 8, along with the corresponding models. The scatter in the resistivity models mirrors the probabilities shown in the PDF plots of Fig. 6, where the vertical resistivity at 1–2 km depth has the least scatter, in association with its tightest probabilities. Conversely, the horizontal resistivity at these depths can be seen to be less well resolved.

In Fig. 9, a number of different scenarios have been subsetted (rows b–d) from the full posterior model distribution (row a). The inline radial electric field has been previously inverted using the Occam method to generate a smooth isotropic 1-D model (Key & Lockwood 2010); this result is shown as the red line in Fig. 9. The Occam inversion model exhibits a smooth resistivity peak in the vicinity of the highest resistivities observed in the Pluto-1 well log. It appears that the highest probability of an interface in the full posterior solution shown in Fig. 9(a) is shallower at close to 2150 m depth. There is another interface probability peak close to 2950 m, although it is of a lower probability. This does not imply that there needs to be interfaces exclusively at one depth or the other, as we shall show with the following analysis.

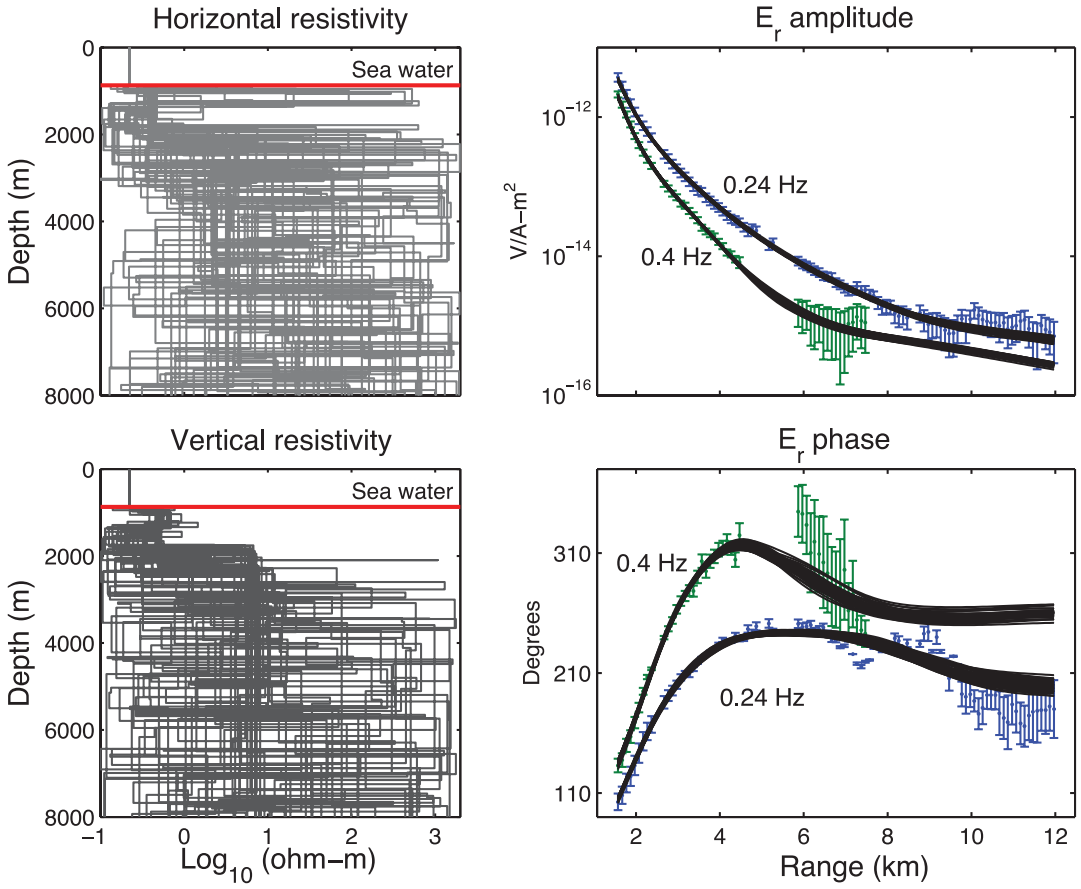

Figure 8. A randomly chosen set of 50 models (left-hand side) fitting to rms 1 from the full posterior model distribution and their data fits (right-hand side). Note how similar the sampled models when plotted together begin to look like the PDFs of resistivity shown in Fig. 6.

Following the same methodology as introduced for the synthetic studies, we look at the posterior distribution of the number of interfaces, and pick out the most probable number, 3. If we only look at this subset of models with exactly three interfaces (wherever they may be) from the final posterior solution ensemble, we obtain the scenario in (b). With this subset the 5 per cent and 95 per cent quantiles become closer in the resistivity PDFs and the probability of an interface near 2150 m depth is now accentuated. 14 per cent of the 94 450 models in the full posterior correspond to this scenario. In (c), we only look at the subset of models from the full posterior ensemble that require interfaces between the depth range 2000 and 2450 m. 77 per cent of the models in the full posterior correspond to this scenario. Note how all these models, which require there to be interfaces between 2000 and 2450 m, also require a high probability of there being interfaces between 2450 and 3300 m. Finally, we could choose to incorporate our knowledge of the nearby well-log which says there is an interface at 3000 m. Or we could also look at it as if we were examining the probability of there being models which require interfaces between 2450 and 3300 m and what features that would require in the rest of the model. Subsetting such models, which require interfaces between 2450 and 3300 m, gives us scenario (d), corresponding to 67 per cent of the models in the full posterior ensemble. Note how there is still a high probability of interfaces at shallower depths between 2000 and 2450 m for all these models. Given that 96 per cent of models require interfaces between 2000 and 3300 m, one can calculate the probability on the number of models that require interfaces to be present in both intervals = (77 per cent + 67 per cent) − 96 per cent = 48 per cent, also borne out by subsetting the full model posterior. Thus 48 per cent of models in the final posterior solution ensemble require there to be interfaces in both intervals, as we set out to demonstrate.

To further illustrate the high-probability scenario (d) shown in Fig. 9, we zoom in to the depths of interest as shown in Fig. 10, where hotter colours correspond to higher probabilities. The Pluto-1 resistivity well log has also been included in the middle panel, and both resistivity panels show the smooth isotropic inversion result from Key & Lockwood (2010). It is encouraging to see that the peak resistivity in the smooth inversion coincides with the high probability value of about 10 ohm-m at around 2950 m depth, as is also suggested by the well log. However, it is rather intriguing that there is a greater probability for another interface near the shallower depth of 2100 m. Given that the isotropic smooth inversion (Key & Lockwood 2010) was regularized with a penalty on model roughness, it is not surprising that this interface was not found given that it would be difficult for such an inversion to resolve a sharp jump in resistivity at depth and the possibility of two or more closely spaced resistive layers.

An explanation may be that the high vertical resistivity at these shallower depths is caused by the presence of regionally extensive shales above the Pluto gas field (Tilbury *et al.* 2009). Shales can exhibit a large vertical resistivity and small horizontal resistivity due to microscopic grain layering and macro scale layer interbedding; since such shales could potentially mask or be mistaken for a resistive hydrocarbon layer,

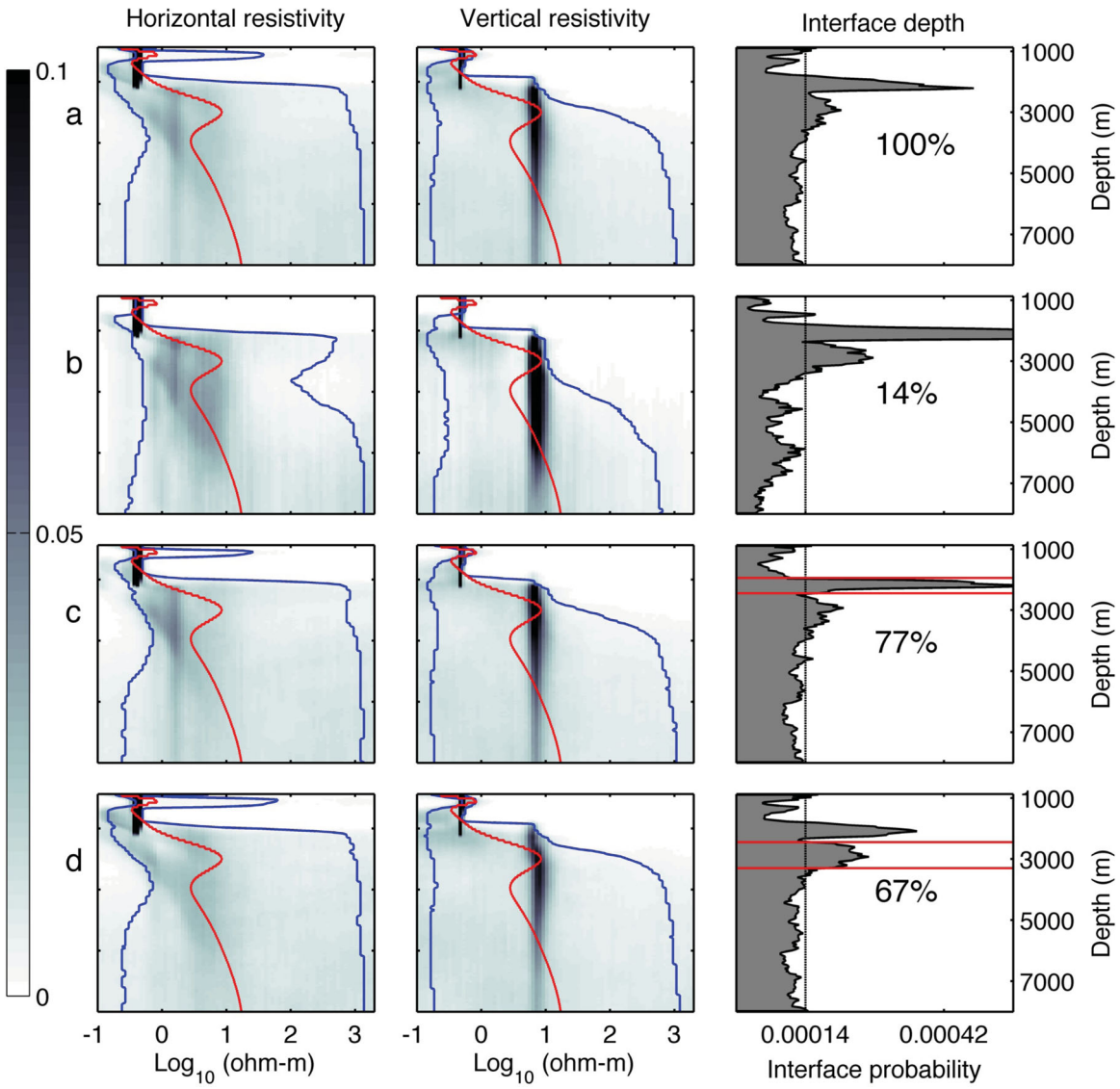

Figure 9. Different scenarios mined from the full posterior ensemble. (a) The full posterior solution and accompanying PDFs. (b) Subset of solutions where the number of interfaces is three (the most probable number). (c) Subset of solutions which require interfaces between 2000 and 2450 m, shown by red horizontal lines. (d) Subset of solutions which require interfaces between 2450 and 3300 m, shown by red horizontal lines. The fraction of models associated with each scenario out of the full posterior are given as percentages in the last column.

the identification of anisotropic shales is of considerable concern for CSEM exploration (e.g. Brown *et al.* 2012). One cannot also discount the possibilities of there being a multilevel reservoir or the reservoir top being shallower in the survey area than in Pluto-1. Finally, this feature could also be the effect of 2-D or 3-D geology, but these possibilities need to be fully modelled by 2-D or 3-D forward solvers to see if the feature is still retained in the resulting posterior distributions. Here our interpretation is limited by having only a single site of relatively noisy data (compared to data from more recent industry surveys). Bayesian analysis of data from additional CSEM receivers located both on and off the Pluto reservoir, along with integration of the stratigraphy determined from seismic imaging and petrophysical analyses from the many nearby wells, would almost certainly shed more light on the nature of the shallower resistive interface detected here.

4 CONCLUSIONS

In this study we have developed a Bayesian approach for the inversion of CSEM data. We used this approach to quantify the resolvability of anisotropic conductivity for a 1-D model representative of an offshore hydrocarbon reservoir, and to quantify the resolution of marine CSEM data collected at the Pluto gas field offshore Northwest Australia.

Our work with synthetic models show that anisotropy can indeed be well resolved in the shallower sediments, at least when the ratio of vertical to horizontal resistivities is near 4:1. Highly resistive isotropic reservoir layers seem to be characterized by very wide distributions with only the peak in the distribution of vertical resistivities at reservoir depth being trustworthy. All field components from the HED except H_z show a similar resolution of the reservoir vertical resistivity, whereas H_z is completely insensitive to the reservoir. The radial inline electric

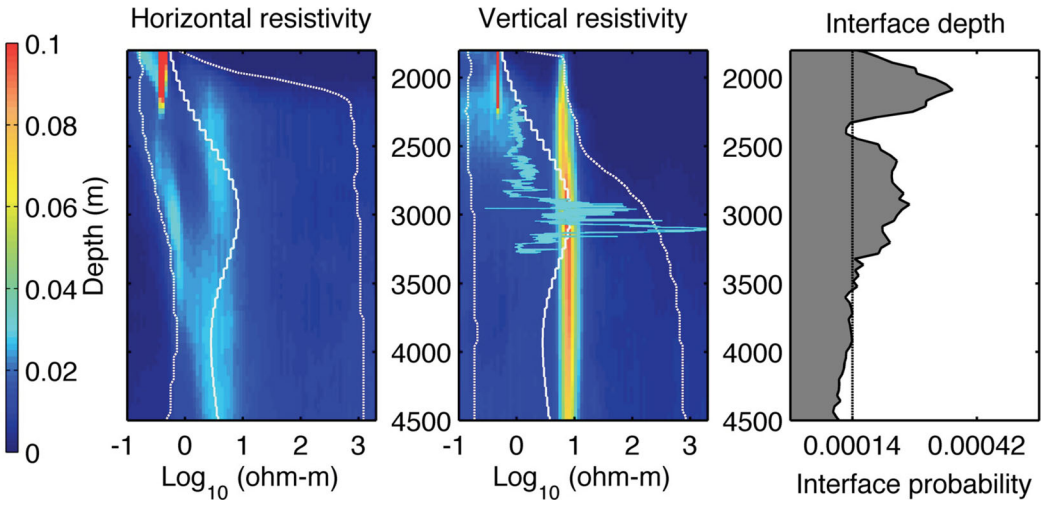

Figure 10. Close up view of scenario (d) from Fig. 9 which requires there to be interfaces between 2450 and 3300 m. In the middle panel, the Pluto-1 well log is shown as the thin blue line. The smooth inversion result from Key & Lockwood (2010) is shown as the thin white line. Hotter colours in the resistivity PDFs represent higher probabilities. Note how the probability of interfaces at shallower depths around 2150 m still remains. The probability of this scenario is 67 per cent.

field E_r seems best at constraining the shallow anisotropy while the vertical electric field E_z seems best at resolving both the reservoir top and bottom depths (Fig. 3). Given that both these field components can be acquired with standard inline geometry, it augurs that with relatively straightforward survey designs over a 1-D target, anisotropy and the reservoir can be resolved if the target geology is not significantly different from what has been studied here.

Our approach to data inversion uses a Bayesian framework and a 'birth–death' RJ-MCMC sampler which has not been used for inverting marine CSEM data yet. The algorithm is trans-dimensional in that the number of model parameters is not fixed *a priori*. Further, the algorithm is self-parametrizing in that the interfaces in a particular model are not fixed to be at a specific location and can move. We differ from other trans-dimensional RJ-MCMC algorithms in mixing a global and local 'update' move for fixed dimension steps instead of using more computationally intensive approaches such as delayed rejection. The algorithm is highly flexible and this method of Bayesian inversion is the most truly 'data driven' approach that the authors have yet converged upon. A further improvement in this direction would be adding the data noise parameters themselves as unknowns (Bodin *et al.* 2012), which would tackle the crucial issue of estimating data noise, which directly affect the misfit function and thus the posterior solution converged upon.

The full posterior ensemble can be subsetted to display model distributions corresponding to a most probable parameter such as the number of interfaces (Bodin *et al.* 2012), to incorporate new information as and when it may become available, or, for hypothesis testing of different plausible geological scenarios. Subsetting is rather easily carried out and does not require additional inversion. Further, different scenarios can be quantitatively compared by the fraction of models required in each scenario out of the total number of models in the full posterior distribution of models.

Application of the trans-dimensional inversion to marine CSEM data from the Pluto field are in general agreement with previous results obtained with smooth inversion. The differences, where they exist, highlight the fact that smooth models which are subjectively regularized to obtain a stable and meaningful result out of the many highly oscillatory ones that all fit the data (Fig. 8)—may miss features that are not smooth variations in resistivity, but nonetheless are likely geological features from a data misfit point of view.

Despite its numerous advantages, an obvious drawback to using this method is the fact that a large number of forward calls need to be made to sample the posterior model distribution adequately. For 1-D earth models, the problem is tractable in that reasonable estimates of the posterior solution can be found within a couple of hours when running on parallel computer systems. The rate limiting step is essentially how long it takes to achieve burn-in for each chain. For Pluto, we ran 128 chains in parallel over 12 hr and oversampled the distribution by at least a factor of two. Post burn-in, if enough chains are run in parallel, the number of further steps required can be reduced if the number of parallel chains is increased. For 2-D or 3-D geology, evaluating a forward model response can take considerably longer and the millions of forward calls may take inordinate amounts of time when done serially. However, given that parallel 2-D and 3-D forward solvers for EM geophysics problems are becoming increasingly more efficient and that independent Markov chains are highly suited to being run in parallel, this bodes well for the future of this flexible Bayesian approach to inverse problem solving.

ACKNOWLEDGMENTS

This work was supported by the Seafloor Electromagnetic Methods Consortium at Scripps Institution of Oceanography. The San Diego Supercomputer Center at UCSD is thanked for providing access to the Triton Compute Cluster. The authors would like to thank G. Michael Hoversten, Bob Nowack, Peter Gerstoft and Eric Lindsey for engaging discussions on convergence criteria for Markov chains. Ross C. Brodie

is thanked for suggestions that helped clarify the text. Anandaroop Ray would like to thank Jan Dettmer and Thomas Bodin for their prompt responses to his myriad queries on the trans-dimensional algorithm and for their advice on its implementation.

REFERENCES

Abubakar, A., Habashy, T.M., Druskin, V.L., Knizhnerman, L. & Alumbaugh, D., 2008. 2.5D forward and inverse modeling for interpreting low-frequency electromagnetic measurements, *Geophysics,* **73**(4), F165–F177.

Agostinetti, N.P. & Malinverno, A., 2010. Receiver function inversion by trans-dimensional monte carlo sampling, *Geophys. J. Int.,* **181**(2), 858–872.

Andriéu, C., de Freitas, N., Doucet, A. & Jordan, M.I., 2003. An introduction to MCMC for machine learning, *Mach. Learn.,* **50,** 5–43, doi:10.1023/A:1020281327116.

Backus, G.E., 1988. Bayesian inference in geomagnetism, *Geophys. J.,* **92**(1), 125–142.

Bayes, T., 1763. An essay towards solving a problem in the doctrine of chances, *Phil. Trans. R. Soc. Lond.,* **53,** 370–418.

Bodin, T. & Sambridge, M., 2009. Seismic tomography with the reversible jump algorithm, *Geophys. J. Int.,* **178**(3), 1411–1436.

Bodin, T., Sambridge, M., Tkalcic, H., Arroucau, P., Gallagher, K. & Rawlinson, N., 2012. Transdimensional inversion of receiver functions and surface wave dispersion, *J. geophys. Res.,* **117**(B02031), 1–24.

Brown, V., Hoversten, M., Key, K. & Chen, J., 2012. Resolution of reservoir scale electrical anisotropy from marine CSEM data, *Geophysics,* **77**(2), E147–E158.

Buland, A. & Kolbjornsen, O., 2012. Bayesian inversion of CSEM and magnetotelluric data, *Geophysics,* **77**(1), E33–E42.

Chen, J., Hoversten, G.M., Vasco, D., Rubin, Y. & Hou, Z., 2007. A Bayesian model for gas saturation estimation using marine seismic AVA and CSEM data, *Geophysics,* **72**(2), WA85–WA95.

Chew, W., 1995. *Waves and Field in Inhomogeneous Media,* Wiley IEEE Press, New York, NY.

Chib, S. & Greenberg, E., 1995. Understanding the metropolis-hastings algorithm, *Am. Stat.,* **49**(4), 327–335.

Collins, M.D. & Fishman, L., 1995. Efficient navigation of parameter landscapes, *Acoust. Soc. Am. J.,* **98,** 1637–1644.

Constable, S., 2010. Ten years of marine CSEM for hydrocarbon exploration, *Geophysics,* **75**(5), 75A67–75A81.

Constable, S.C. & Weiss, C.J., 2006. Mapping thin resistors and hydrocarbons with marine EM methods: insights from 1D modeling, *Geophysics,* **71**(2), G43–G51.

Constable, S.C., Parker, R.L. & Constable, C.G., 1987. Occam's inversion - a practical algorithm for generating smooth models from electromagnetic sounding data, *Geophysics,* **52**(03), 289–300.

Dettmer, J., Dosso, S. & Holland, C., 2010. Trans-dimensional geoacoustic inversion, *J. acoust. Soc. Am.,* **128,** 3393–3405.

Dosso, S.E. & Dettmer, J., 2011. Bayesian matched-field geoacoustic inversion, *Inv. Probl.,* **27**(5), 055009, doi:10.1088/0266-5611/27/5/055009.

Ellingsrud, S., Eidesmo, T., Johansen, S., Sinha, M.C., MacGregor, L.M. & Constable, S., 2002. Remote sensing of hydrocarbon layers by seabed logging (SBL): results from a cruise offshore Angola, *Leading Edge,* **21,** 972–982.

Green, P., 1995. Reversible jump MCMC and Bayesian model selection, *Biometrika,* **82,** 711–732.

Gunning, J., Glinsky, M.E. & Hedditch, J., 2010. Resolution and uncertainty in 1D CSEM inversion: a Bayesian approach and open-source implementation, *Geophysics,* **75**(6), F151–F171.

Hastings, W.K., 1970. Monte carlo sampling methods using markov chains and their applications, *Biometrika,* **57**(1), 97–109.

Hou, Z., Rubin, Y., Hoversten, G.M., Vasco, D. & Chen, J., 2006. Reservoir-parameter identification using minimum relative entropy-based Bayesian inversion of seismic AVA and marine CSEM data, *Geophysics,* **71**(6), O77–O88.

Huelsenbeck, J.P., Larget, B. & Alfaro, M.E., 2004. Bayesian phylogenetic model selection using reversible jump Markov chain Monte Carlo, *Mol. Biol. Evol.,* **21**(6), 1123–1133.

Key, K., 2009. 1D inversion of multicomponent, multifrequency marine CSEM data: methodology and synthetic studies for resolving thin resistive layers, *Geophysics,* **74**(2), F9–F20.

Key, K., 2012a. Is the fast Hankel transform faster than quadrature? *Geophysics,* **77**(3), F21–F30.

Key, K., 2012b. Marine electromagnetic studies of seafloor resources and tectonics, *Surv. Geophys.,* **33**(1), 135–167.

Key, K. & Lockwood, A., 2010. Determining the orientation of marine CSEM receivers using orthogonal procrustes rotation analysis, *Geophysics,* **75**(3), F63–F70.

Li, Y. & Dai, S., 2011. Finite element modelling of marine controlled-source electromagnetic responses in two-dimensional dipping anisotropic conductivity structures, *Geophys. J. Int.,* **185,** 622–636.

Liang, F., Liu, C. & Carrol, R.J., 2010. *Advanced Markov Chain Monte Carlo Methods: Learning from Past Samples,* Wiley Series in Computational Statistics, Wiley, New York, NY.

Løseth, L.O. & Ursin, B., 2007. Electromagnetic fields in planarly layered anisotropic media, *Geophys. J. Int.,* **170**(1), 44–80.

Malinverno, A., 2002. Parsimonious Bayesian Markov chain Monte Carlo inversion in a nonlinear geophysical problem, *Geophys. J. Int.,* **151,** 675–688.

Minsley, B.J., 2011. A trans-dimensional Bayesian Markov chain Monte Carlo algorithm for model assessment using frequency-domain electromagnetic data, *Geophys. J. Int.,* **187**(1), 252–272.

Neal, R.M., 2003. Slice sampling, *Ann. Stat.,* **31**(3), 705–767.

Newman, G.A. & Alumbaugh, D.L., 2000. Three-dimensional magnetotelluric inversion using non-linear conjugate gradients, *Geophys. J. Int.,* **140**(2), 410–424.

Ramananjaona, C., MacGregor, L. & Andréis, D., 2011. Sensitivity and inversion of marine electromagnetic data in a vertically anisotropic stratified earth, *Geophys. Prospect.,* **59**(2), 341–360.

Scales, J.A. & Snieder, R., 1997. To Bayes or not to Bayes?, *Geophysics,* **62**(4), 1045–1046.

Sen, M. & Stoffa, P.L., 1995. *Global Optimization Methods in Geophysics,* Elsevier, Amsterdam.

Smith, K., Gatica-Perez, D. & Odobez, J.-M., 2005. Using particles to track varying numbers of interacting people, in *Proceedings of IEEE Computer Society Conference on Computer Vision and Pattern Recognition (CVPR),* Vol. 1, pp. 962–969, San Diego, CA.

Tarantola, A., 2005. *Inverse Problem Theory and Methods for Model Parameter Estimation,* Society of Industrial and Applied Mathematics, Philadelphia, PA.

Tilbury, L.A. *et al.*, 2009. Pluto - a major gas field hidden beneath the continental slope (dvd), *APPEA J.,* **49,** 243–265.

Tompkins, M.J., Fernández Martínez, J.L., Alumbaugh, D.L. & Mukerji, T., 2011. Scalable uncertainty estimation for nonlinear inverse problems using parameter reduction, constraint mapping, and geometric sampling: marine controlled-source electromagnetic examples, *Geophysics,* **76**(4), F263–F281.

Trainor-Guitton, W. & Hoversten, G.M., 2011. Stochastic inversion for electromagnetic geophysics: practical challenges and improving convergence efficiency, *Geophysics,* **76**(6), F373–F386.

Um, E.S. & Alumbaugh, D.L., 2007. On the physics of the marine controlled-source electromagnetic method, *Geophysics,* **72**(2), WA13–WA26.